

Final Performance Report

Multifunctional Magnetic Nanowires for Biomagnetic Interfacing Concepts

AFOSR Agreement Number F49620-02-1-0307

July 14, 2006

Reporting Period: June 15, 2002 – December 15, 2005

Principal Investigator: Daniel H. Reich

Address: Johns Hopkins University
Department of Physics and Astronomy
3400 North Charles Street
Baltimore, MD 21218

REPORT DOCUMENTATION PAGE			<i>Form Approved</i> OMB No. 074-0188	
Public reporting burden for this collection of information is estimated to average 1 hour per response, including the time for reviewing instructions, searching existing data sources, gathering and maintaining the data needed, and completing and reviewing this collection of information. Send comments regarding this burden estimate or any other aspect of this collection of information, including suggestions for reducing this burden to Washington Headquarters Services, Directorate for Information Operations and Reports, 1215 Jefferson Davis Highway, Suite 1204, Arlington, VA 22202-4302, and to the Office of Management and Budget, Paperwork Reduction Project (0704-0188), Washington, DC 20503				
1. AGENCY USE ONLY (Leave blank)		2. REPORT DATE	3. REPORT TYPE AND DATES COVERED Final report covering 06/15/02 -12/15/05	
4. TITLE AND SUBTITLE Multifunctional Magnetic Nanowires for Biomagnetic Interfacing Concepts			5. FUNDING NUMBERS F49620-02-1-0307	
6. AUTHOR(S) D. H. Reich, C. S. Chen, C. L. Chien, G. J. Meyer, K. Leong, P. C. Searson, G. Xiao				
7. PERFORMING ORGANIZATION NAME(S) AND ADDRESS(ES) Johns Hopkins University 3400 N. Charles St. Baltimore, MD 21218			8. PERFORMING ORGANIZATION REPORT NUMBER	
9. SPONSORING / MONITORING AGENCY NAME(S) AND ADDRESS(ES) AFOSR			10. SPONSORING / MONITORING AGENCY REPORT NUMBER AFRL-SR-AR-TR-06-0271	
11. SUPPLEMENTARY NOTES				
12a. DISTRIBUTION / AVAILABILITY STATEMENT Approved for Public Release				12b. DISTRIBUTION CODE
13. ABSTRACT (Maximum 200 Words) A technique of increasing importance in biotechnology is the manipulation of cells and biomolecules with small magnetic particles. In this research program, we developed a new type of carrier particle, multifunctional magnetic nanowires, which possess tunable magnetic and chemical properties. These nanowires can carry out multiple tasks e.g. binding multiple types of molecules, probing chemical activity in specific regions of a cell, and responding to light as well as to magnetic fields. Among the DoD relevant applications envisioned for the nanowires are new techniques for biosensing, novel approaches to tissue engineering, and a variety of diagnostic and therapeutic approaches including rapid drug delivery, gene therapy and high-efficiency cell sorting. This program carried out the development steps necessary to demonstrate the feasibility of these applications.				
14. SUBJECT TERMS				15. NUMBER OF PAGES
				16. PRICE CODE
17. SECURITY CLASSIFICATION OF REPORT	18. SECURITY CLASSIFICATION OF THIS PAGE	19. SECURITY CLASSIFICATION OF ABSTRACT	20. LIMITATION OF ABSTRACT	

1. Statement of Objectives.

The integration of biology and the physical sciences at the nanoscale has the potential to revolutionize many areas of science and technology. The nanometer size scale is a crucial one, as the dimensions of large biomolecules such as proteins and DNA, as well as those of many important sub-cellular structures, fall in this range. Recent advances in materials research have made it possible to engineer materials on these same nanometer lengthscales, and thus it is now possible to begin to design devices and artificial structures that can interact with cells and biomolecules in fundamentally new ways.

A technique of increasing importance in biotechnology is the manipulation of cells and biomolecules with small magnetic particles. In this research program, we set out to develop a new type of carrier, multifunctional magnetic nanowires, which possess tunable magnetic and chemical properties. These nanowires can carry out multiple tasks e.g. binding multiple types of molecules, probing chemical activity in specific regions of a cell, and responding to light as well as to magnetic fields. Among the DoD relevant applications envisioned for the nanowires are new techniques for biosensing, novel approaches to tissue engineering, and a variety of diagnostic and therapeutic approaches including rapid drug delivery, gene therapy and high-efficiency cell sorting. The goal of this program was to carry out the development steps necessary to demonstrate the feasibility of these applications.

The specific research objectives included:

Selective Functionalization. Development of a toolkit of robust and stable molecule-surface linkages that can selectively bind to multi-segmented nanowires.

Tuning Magnetic Properties of Nanowires. Exploration of designs of nanowires for efficient transport, collection and the application of force; investigation of the magnetic properties of multi-segment nanowire architectures for applications such as rapid cell sorting and scaffolds for tissue engineering.

Cell-Nanowire Interactions. Elucidation of cell-nanowire interactions, including specific cell-surface receptor binding, directed internalization, and transfection.

Assembly of Multi-Nanowire Structures. Development of techniques to control the magnetic and/or chemically driven self-assembly of multifunctional nanowires, and the study of cell proliferation, differentiation and tissue deposition on these scaffolds.

Manipulation of Cells and Molecules. Development of methods that use nanowires to manipulate both large populations of cells, and individual cells using combinations of lithographically patterned micro-magnets and externally applied magnetic fields.

New Biosensing Strategies using Nanowires. Investigation of novel approaches to magnetic biosensing using magnetic nanowires, and studies of the potential of these strategies for both low-field and multiplexing assays.

2. Status of effort.

In the course of this program, we made significant progress toward addressing the

challenges that must be met to develop multifunctional magnetic nanowires for biomagnetic applications. These include (i) tuning of magnetic and other physical properties of nanowires, (ii) selective functionalization and biocompatibility, (iii) manipulation and positioning of cells with nanowires, (iv) nanowire self-assembly in 1D, 2D, and 3D, (v) control of nanowire-cell interactions, (vi) transport through cell membrane using nanowires, and (vii) developing magnetic sensing strategies for nanowires. Results are described in detail in Section 3 below. These include nanowire functionalization, controlling the behavior of nanowires in liquid suspension, enhanced performance in magnetic trapping applications, new approaches to magnetic cell trapping, assembly of multi-nanowire constructs, demonstration of both in vitro and in vivo gene delivery with nanowire carriers, magnetic detection of nanowires for biosensing applications, and extensions of the multifunctional magnetic nanoparticle concept to other particle geometries.

3. Accomplishments/New Findings.

3.1 Nanowire functionalization

Selective Functionalization of Magnetic Nanowires: Gold, nickel, and two-segment gold-nickel nanowires have been synthesized by electrodeposition into nanoporous alumina templates. The wires have ~ 350 nm diameters and were typically 8-15 microns in length. The nanowires were removed from the templates and were functionalized with organic molecules. Adsorption isotherms were constructed for the binding of [8,13-bis(1-hydroxyethyl)-3,7,12,17-tetra-methyl-21 *H*,23 *H*-porphine-2,18-dipropionic acid] to nickel nanowires in ethanol solution at 298 K. Adduct formation constants of $9 \pm 5 \times 10^6 \text{ M}^{-1}$ and limiting surface coverages of $8 \times 10^{-10} \text{ mol/cm}^2$ were abstracted from the isotherms. Surface functionalization conditions were identified where thiols bind selectively to gold and carboxylic acids bind to the nickel. Coupling of fluorescent dyes to nanowires with free amino or thiol functional groups was quantified by fluorescence microscopy. These reactions with two-segment gold-nickel nanowires produced materials that emitted light only on one segment of the wire or different colors of light on each segment [Publication 1].

Selective Binding of Proteins to Two-Segment Magnetic Nanowires. Metallic nanowires composed of nickel and gold as well as bimetallic nickel-gold nanowires were fabricated via templated electrodeposition. Gold surfaces were functionalized with alkanethiols with terminal hexa(ethylene glycol) groups, while nickel surfaces were functionalized with palmitic acid, a 16-carbon fatty acid. When combined with a fluorescent-tagged protein, hydrophobic nickel wires exhibited bright fluorescence while EG₆-terminated gold wires did not, indicating that the protein did not adhere to the EG₆-functionalized nanowires. Nickel-gold nanowires presenting distinct segments of alkyl and EG₆ surfaces were also combined with the fluorescent protein. Intense fluorescence was only observed on the nickel segment of these wires, demonstrating that proteins selectively adsorbed to one portion of these multisegment nanostructures [Publication 2].

In further work, we increased our ability to selectively functionalize two-segment nanowires with hydrophobic and hydrophilic groups for the selective adsorption of proteins and for directed internalization by mammalian cells. Shown in Figure 5-2005 are idealized representations of two segment nickel-gold (Ni-Au) nanowires we have

recently prepared. Our findings enable us to use molecular functionality to direct proteins to the nickel or to the gold segment.

On the right hand side of Figure 1 is a nickel-gold nanowire with a hydrophobic nickel end and a hydrophilic gold end. The left hand side shows the inverse structure, i.e.

hydrophilic nickel and hydrophobic gold. The synthesis of the molecular ligands that impart the hydrophobic/hydrophilic nature are described in *Publication 19*. In general, methyl terminated ligands give rise to hydrophobic surfaces and (are thus abbreviated NiCH_3 , or AuCH_3) and polyethylene glycol groups yield hydrophilic surfaces (NiEG_6 or AuEG_6).

The adsorption of fluorescently-labeled IgG proteins to the surfaces of these nanowires was studied by fluorescence and optical microscopy. For comparison, functionalized single component nickel and gold wires were also reacted with the fluorescent protein to contrast the degree of protein adsorption on hydrophobic and hydrophilic nanowire surfaces. In general, Ni-Me nanowires showed bright fluorescence while Au-EG nanowires were very dim or completely non-fluorescent (Figure 2). Since there appeared to be a significant distribution of fluorescence intensities for both the NiCH_3 and AuEG_6 wires, a quantitative analysis was also carried out.

When bifunctional $\text{NiCH}_3\text{-AuEG}_6$ nanowires were combined with the fluorescent antibody, selective adsorption of the protein to the hydrophobic nickel segment was observed. Several representative images are shown in Figure 3. In the upper row, reflection images show the two distinct nanowire segments, where gold is the shiny section and nickel is the more dull section. The bottom row contains the corresponding fluorescence images of the same nanowires. In each set of images, it is clear that only the nickel portion of the nanowire is fluorescent, indicating the presence of protein on only the hydrophobic segment. Bifunctional $\text{NiEG}_n\text{-AuCH}_3$ wires exhibited the same behavior; protein was selectively adsorbed onto the hydrophobic gold segment..

3.2 Tuning the magnetic properties of nanowires.

Tuning the response of magnetic suspensions: In contrast to the spherical particles commonly used in biomagnetic applications, rod-shaped particles such as nanowires exhibit additional degrees of freedom that are associated with their inherent shape

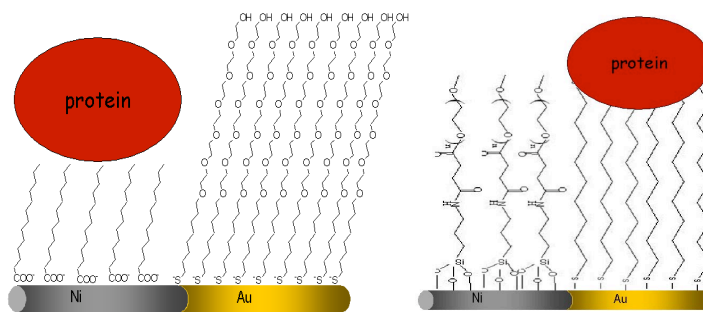


Figure 1. Selective protein adsorption to a distinct segment of a two-component nanowire.

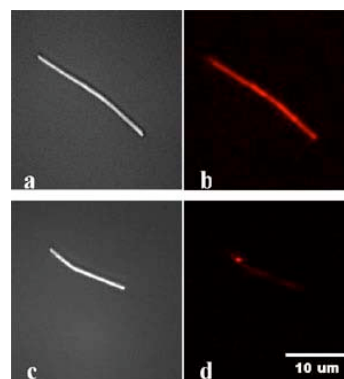


Figure 2. Protein adsorption to single component nanowires (a) Reflection image of NiCH_3 nanowire after reaction with fluorescent protein. (b) Fluorescence image of same nanowire. (c) Reflection image of AuEG_6 nanowire after reaction with fluorescent protein. (d) Fluorescence image of same nanowire.

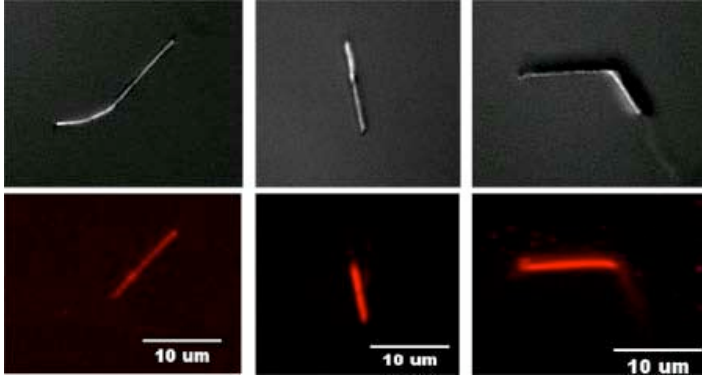


Figure 3. Selective adsorption of protein to bifunctional nanowires. Upper row: Reflection images of three $\text{Ni}_1\text{CH}_3\text{-AuEG}_6$ nanowires which have been combined with fluorescent protein. The darker segment is nickel and the brighter segment is gold. Bottom row: Corresponding fluorescence images, showing protein adsorption localized on the nickel segment.

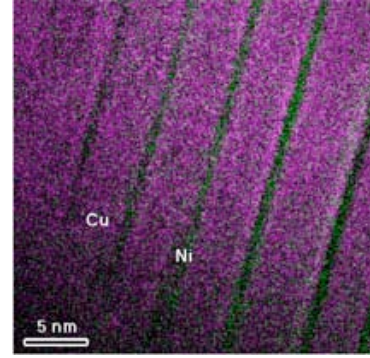


Figure 4. TEM EELS image of part of a $[\text{Ni}(1.5 \text{ nm})/\text{Cu}(4 \text{ nm})]$ $d = 30 \text{ nm}$ nanowire with disk-shaped magnetic Ni segments.

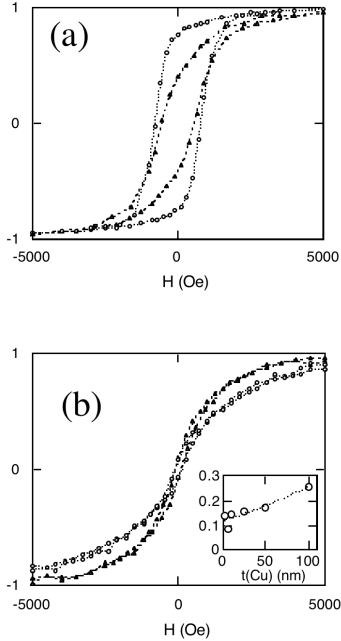


Figure 5. $M - H$ loops for arrays of Ni/Cu multilayer nanowires (a) $[\text{Ni}(125 \text{ nm})/\text{Cu}(125 \text{ nm})]_{10}$, $d = 50 \text{ nm}$, and (b) $[\text{Ni}(5 \text{ nm})/\text{Cu}(5 \text{ nm})]_{250}$, $d = 50 \text{ nm}$. In (a) the nanowires have rod shaped FM segments (aspect ratio 2.5) and the easy axis is parallel to the wire axis. In (b) the nanowires have disk shaped FM segments (aspect ratio 0.1) and the easy axis is perpendicular to the wire axis. The inset shows the remanence for $[\text{Ni}(5 \text{ nm})/\text{Cu}(X \text{ nm})]$ $d = 50 \text{ nm}$ nanowires as a function of the thickness of the copper layer.

anisotropy. Furthermore, the introduction of multiple components along the length of a nanowire can lead to further degrees of freedom associated with the magnetic coupling between the layers. By modifying the diameter, composition, and layer thicknesses in multilayer nanowires it is possible to control the orientation of the magnetic easy axis and to tailor properties such as the coercivity, saturation field, saturation magnetization, remanent magnetization, and the Curie temperature. We have shown that the magnetic shape anisotropy and dipolar interactions between magnetic layers can be exploited to tailor the magnetic response in ferromagnetic/nonmagnetic (FM/NM) multilayer nanowires in a suspension.

Copper/nickel multilayer nanowires with either disk-shaped or rod-shaped magnetic Ni segments (Figure 4) were fabricated by electrochemical deposition from a solution containing both nickel and copper ions. For rod shaped magnetic segments the easy axis is parallel to the nanowire axis [Figure 5(a)]. The segments are single domain in this size regime and exhibit large coercivity and remanence due to the inherent shape anisotropy and reduced dimensions. In contrast, the axis perpendicular to the nanowire axis is the magnetic hard axis with small coercivity and remanence.

For wires with disk-shaped segments, the magnetic easy axis is perpendicular to the nanowire axis and the hard axis is parallel to the nanowire axis [Figure 5(b)]. The remanence is very small due to the dipolar interactions between adjacent FM layers. The remanence can be tuned by adjusting the copper layer thickness. Dipolar interactions between the magnetic segments favor antiparallel alignment of the domains in adjacent nickel segments. As the copper layer thickness increases, the remanence increases as the dipolar interactions become weaker.

These properties can be exploited in a variety of ways. For example, in fluid suspension, the different easy axes of the rod-segmented and disk-segmented wires causes them to align respectively parallel and perpendicular to an applied magnetic field.

These results are described in more detail in *Publications 3 and 14*.

Synthesis of Metal Oxide Nanowires Nanowires composed of a variety of metal oxide materials have been synthesized. TiO_2 and ZnO nanowires have been fabricated by sol-gel methods as well as by electrodeposition. When excited by UV light, ZnO nanowires exhibit a characteristic yellow-green emission. Magnetic iron oxide nanowires have also been synthesized by electrodeposition. Multi-component nanowires which incorporate metallic and metal oxide segments have also been fabricated, including gold-iron oxide and Ni-TiO_2 . These latter nanowires have potential applications as magnetic beacons in a variety of intracellular applications.

3.3 Magnetic Cell Separations

One of the most important applications of magnetic particles in biology is magnetic separation. In this process magnetic particles are bound to one or more components of a heterogeneous mixture of cells or biomolecules. To develop methods of cell manipulation with magnetic nanowires, we conducted magnetic cell separation studies, on cultures of NIH-3T3 mouse fibroblast cells, using single-component ferromagnetic Ni nanowires, with diameters of 350 nm, and lengths between 5 μm and 40 μm . The outperform the beads in both one-step and three-step separation procedures [Publication 5].

We subsequently explored the mechanism of those interactions, focusing on the effects of changing nanowire length relative to cell size in magnetic separations. After seeding nanowires over a culture of adherent NIH-3T3 cells, the cells were found to bind to the nanowires through integrin receptors, as indicated by the formation of focal adhesions along the length of the nanowires. This process occurred quickly (< 1 h) and the cells were found to internalize even the largest nanowires. By 24 hours, nearly all of the nanowires were internalized and appeared to be in the cytoplasm rather than in a lipid vesicle, as observed by transmission electron microscopy (TEM). Following introduction of the nanowires into the cell culture, the cells were detached from the substrate, and the suspension of cells was separated in a magnetic field. Nanowires were found to generate high-purity separations over a considerable range of nanowire sizes. Interestingly, we found that the separation yield was optimized when the

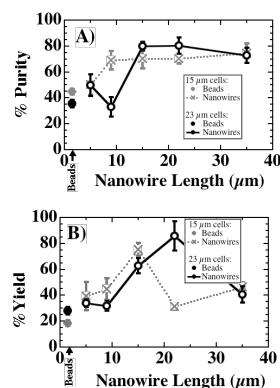


Figure 6. (A) Percent purity vs nanowire length and (B) Percent yield vs nanowire length for separations using 15 μm and 23 μm diameter cells

nanowires' length corresponded to the average diameter of the suspended cells, indicating strong length dependence to the cell-nanowire interaction process (Figure 6). When the average cell diameter was changed within the same cell line, the optimal nanowire length changed accordingly. By performing a magnetic separation on a cell population with a bimodal size distribution, we were able to selectively capture the cells with larger diameter, as shown in Figure 7, suggesting the potential use of nanowires to magnetically separate cell populations by size through control of the geometry of the wires.

We subsequently carried out fluorescence imaging studies that establish both the mechanism of cell-nanowire binding/internalization, and the source of the peak in the yield [Publication 15]. Previous studies have shown that fibroblast cells take up magnetic beads by first forming focal adhesions on the particles before internalization. These focal adhesions formed by the cell during phagocytosis are specialized structures which contain high concentrations of many proteins, including, amongst others, actin and paxillin. Immunofluorescence microscopy of cells exposed to nanowires confirms that the cells also internalize the nanowires through a similar integrin-mediated phagocytosis. Cells exposed to nanowires were fixed and stained for filamentous actin and paxillin localization at various times following exposure. As seen in Figures 8A and 8B, the cells interact with the nanowires by forming focal adhesions along the length of the nanowire as shown by the discrete concentrations of paxillin which cluster on the nanowire. Actin is also concentrated along the length of these nanowires. At 30 minutes, these focal adhesions are clearly present, but they disappear within 24 hours, suggesting that the cells have internalized the nanowires. To provide direct confirmation that nanowires were being internalized on this timescale, nanowires were coated with mouse IgG protein before incubation with the cells, exposed to the cells, and fixed and stained with fluorescently-tagged anti-mouse antibodies. As illustrated in Figures 8C and 8D, after 30 minute incubation with the IgG-coated nanowires, the nanowires are detected by the fluorescent anti-mouse antibody, and are therefore external to the cells. However, after 24 hours, the nanowires are protected from the fluorescent stain as seen in Figures 8E and 8F and have thus been internalized by the cells. Quantifying these results, we found that the percent of nanowires internalized increased with time from 10% at 30 minutes to 70% at 24 hours. To further characterize which subcellular compartment the internalized nanowires were taken into, cells incubated with nanowires for 24 hours were fixed, sectioned, and prepared for TEM analysis. Figure 8G is a TEM image of a cell incubated with a nanowire for 24 hours, where the section has been made perpendicular to the long axis of the nanowire to show it

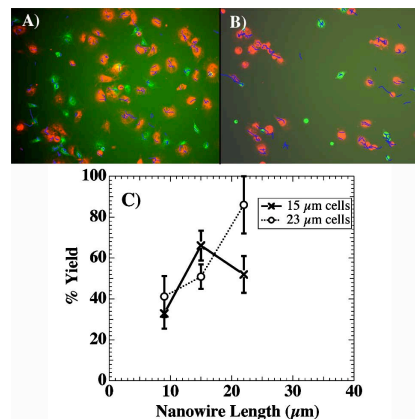


Figure 7. Magnetic separation of heterogeneous cell culture using 22 μm nanowires. Cells treated with mitomycin-C-treated to increase their average diameter to 23 μm are stained red, the untreated cells (average diameter = 15 μm) are stained green, and nanowires are shown in blue. (A) Initial population, (B) Captured cell population, and (C) percent yield vs nanowire length of separations of heterogeneous cultures of 15 and 23 μm diameter cells.

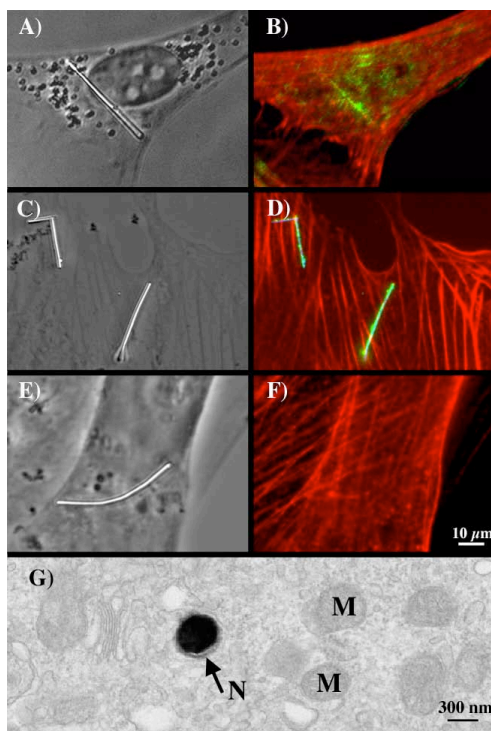


Figure 8. Binding of cell to nanowire (A) cell incubated with a 35 μm nanowire for 30 minutes. (B) composite fluorescent image of the same cell showing actin filaments (red) and paxillin focal adhesions (green). (C) cell after a 30 minute incubation with mouse IgG coated nanowires. (D) composite fluorescence image of the same cell showing actin filaments (red) and immunofluorescent staining of mouse IgG (green) on the nanowire, indicating that the nanowire is external to the cell. (E) cell after a 24 hour incubation with mouse IgG coated nanowires and (F) composite fluorescence image of the same cell showing actin filaments (red) only. The mouse IgG on the nanowire is unstained, indicating that the nanowire is internalized. (G) TEM image of a cell incubated with a nanowire for 24 hours; N: nanowire, M: mitochondria.

of a 15 μm diameter cell with a 22 μm long nanowire is shown in Figure 9E, which confirms that the nanowire is external to the cell. These studies suggest that the longer nanowires are indeed protruding out of the cell, and this exposed section of the nanowire may be more susceptible to influences of mechanical stresses which could more easily remove the nanowire from the cell. This may constitute the basis for how the cells lose the long nanowires during the separation process, although further investigation of this phenomenon is necessary to reach a definitive conclusion.

in a cross-sectional view. The nanowires were found with a lipid bilayer envelope, indicating that the nanowires are trafficked into the cytoplasmic compartment.

To investigate whether the yield peak results from cells releasing the longer nanowires during the separation process, we repeated the internalization study on cells that were first incubated with IgG-coated nanowires for 24 hours and then detached and suspended by exposure to trypsin. We found that because the cells in suspension form spheres, they interact with the nanowires differently depending on whether the length of the nanowire is longer or shorter than the diameter of the suspended cells. For example, Figures 9A and 9B are transmitted light and fluorescent images of two 9 μm nanowires, one which is freely floating and one which is attached to a suspended cell. We found that nanowires that were free from cells were stained by the dye, whereas nanowires associated with cells were protected from the fluorescent stain and hence were still internal to the cell. Therefore, when the cells were attached to nanowires with lengths smaller than their diameter, the nanowire could remain enclosed by the cell even when detached from the substrate. In contrast, as shown in Figures 9C and 9D, when the nanowire length was larger than the diameter of the suspended cells, the nanowire was no longer protected from the stain. We observed that 75% of the suspended cells showed fluorescence on the portion of the nanowire that appeared to be outside of the cell. However, for 25% of the suspended cells that were bound to long nanowires, the entire length of the nanowire stained. An SEM image

3.4 Multicellular Constructs and Magnetic Trapping of Cells

We have developed an approach for controlling the spatial organization of mammalian cells using ferromagnetic nanowires in conjunction with patterned micromagnet arrays (*Publication 16*). As shown in Figure 10, diverse array geometries composed of thin film, ellipsoidal permalloy micromagnets were produced by photolithography. When cells bound to magnetic nanowires flow over these arrays, the magnetic fields produced by these arrays can be used together with small externally applied fields to control the positioning of the cells. Through magnetic forces on the bound wires, the cells are pulled into regions of strong local field, and as shown in Figs. 10(a)-(f), both individual cells and ordered collections of cells can be achieved. In designing such structures, accurate prediction of device performance can be obtained by maps of the magnetic energy $U = -\mu \cdot B$ of the nanowires over the arrays. Figures 10(g)-(o) show U for these arrays. Figures 10(g)-(i) show grayscale maps at a height $z = 8 \mu\text{m}$ above the arrays where far-field wire-array interactions determine the large-scale features of the trapped cell patterns. The wires and cells are repelled from the regions shown in white, and attracted to the dark areas. The detailed positioning is determined by short-range wire-micromagnet interactions. This is illustrated by the energy maps on vertical cuts over the arrays shown in Figs. 10(j)-(o).

Further control of the cell arraying process is obtained by varying the direction and strength of the fluid flow over the arrays, or by reversing the direction of the applied external field, which can cause the cells to land on top of the micromagnets, rather than at their ends. These experiments demonstrated the possibility of using magnetic nanowires to organize cells.

Heterotypic Magnetic Cell Trapping Building on the above results, we have begun developing techniques to trap multiple cell types in controlled proximity. Our approach uses vertical magnetic fields to orient the nanowires, and thereby to direct them to one end of holes patterned in magnetic thin films (Figure 11). The holes provide well-defined magnetic poles for trapping, and allow convenient visualization of the trapped cells. Chemical functionalization of the surface is then used to confine the trapped cells to the regions of the holes. A second cell type may then be introduced by reversing the magnetic field, which then directs them to the unoccupied ends of the holes. This has the

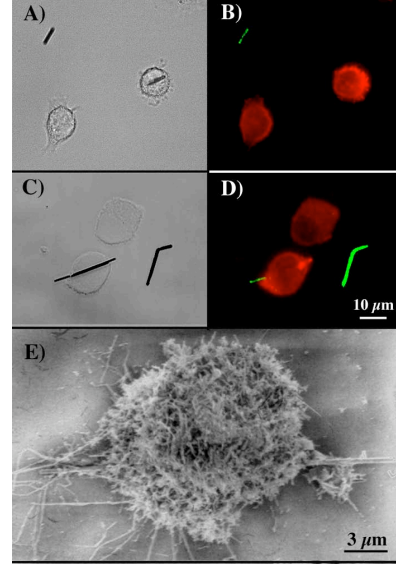


Figure 9. Optical images of suspended 3T3 cells. Top row: Suspended cell bound to a $9 \mu\text{m}$ mouse IgG-coated nanowire. (A) Transmitted light and (B) composite fluorescence image of the same cell showing actin filaments (red) and staining of the mouse IgG (green) on an isolated nanowire (upper left), but not on the bound nanowire which is in the cell. Second row: Suspended cell bound to a $22 \mu\text{m}$ mouse IgG-coated nanowire. (C) Transmitted light and (D) composite fluorescence image of the same cell showing actin filaments (red) and staining of the mouse IgG on both the portion of the nanowire which is no longer internal to the cell and on an isolated nanowire (right). (E) SEM image of a suspended cell bound to a $22 \mu\text{m}$ nanowire

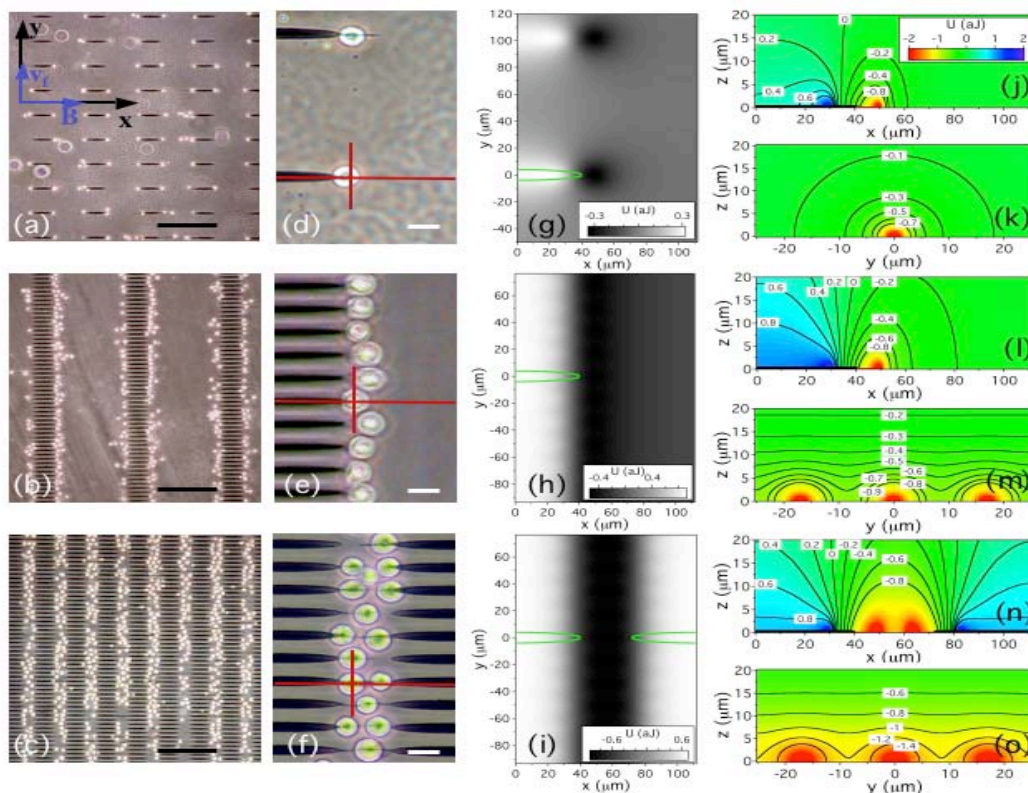


Figure 10. (a)-(c) Overview images of cell positioning on magnetic arrays. The direction of the external field $B = 10 \text{ mT}$ and the fluid flow v_f are shown in (a). Scale bars in (a)-(c) = $200 \mu\text{m}$. (d)-(f) Close-up images of panels (a)-(c). Scale bars in (d)-(f) = $20 \mu\text{m}$. (g)-(i) Calculated magnetic energy for a cell with a wire at a height $z = 8 \mu\text{m}$ above the regions shown in (d)-(f). The wire is attracted to dark regions, and repelled from white regions. Selected micromagnets are outlined in green. (j)-(o) Calculated magnetic energy of wire and cell in vertical planes above the red lines in (d)-(f). The micromagnets appear as thick black lines at the bottom of (j), (l), and (n). Attractive regions appear in red.

potential to enable controlled heterotypic cell trapping, with significantly improved efficiency compared to that achieved by chemical patterning alone. Such devices have potential applications for quantitative studies of cell-cell interactions with relevance to areas such as angiogenesis and wound healing. Further work on improving this technique is continuing beyond the funding period of the present grant.

3.5 Assembly of Nanowire Constructs

Receptor-mediated Self-Assembly: The bottom up approach to device fabrication involves the synthesis and assembly of nanoscale building blocks. Assembly is usually achieved through electrostatic or chemical interactions between the individual building blocks or through interaction with an external electric or magnetic field. In more sophisticated approaches, the building blocks can be functionalized with molecules whose end groups will only bind specifically to other particles functionalized with a complementary functional group. Such receptor mediated interactions have been exploited for the self-assembly of spherical nanoparticles. The assembly of more complex structures requires the ability to control the shape, composition, and surface chemistry of the building blocks. Multicomponent particles, such as multisegment

nanowires, allow the possibility of attaching different functional groups to different segments thereby providing spatially localized functionality. This feature is particularly attractive for self-assembly since receptor groups can be attached at specific locations on the particle where attachment will occur. Directed assembly using receptor mediated interactions provides a powerful tool for the self-assembly of complex architectures.

In exploiting receptor mediated assembly, it is desirable to understand the dynamics of the assembly process so that parameters such as chain length can be predicted for any arbitrary set of experimental conditions. Directed end-to-end assembly of nanowires represents a simple model system to explore the dynamics of receptor mediated self-assembly (*Publication 18*).

The building blocks in these experiments were three segment Au/Ni/Au nanowires prepared by electrochemical template synthesis. The nanowires were 300 nm in diameter and about 4.5 μm long with 10 nm gold end-segments. The short gold end-segments with an aspect ratio of about 0.03 maximize the probability of attachment at the end faces of the cylinders. The functionalization scheme for directed end-to-end assembly using the biotin-avidin linkage was as follows. The biotin was attached to the gold end-segments through a thiol group forming a self-assembled monolayer. The biotin-terminated thiol includes a tetra(ethylene oxide) spacer group between the biotin and the alkane chain to provide greater hydrophilicity and flexibility for the ligand-receptor interaction. Non-specific binding of the biotin-terminated thiol to the central segments was prevented by first attaching palmitic acid ($\text{CH}_3(\text{CH}_2)_{14}\text{CO}_2\text{H}$), a short chain carboxylic acid that binds selectively to the native oxide on the nickel. A separate suspension of biotin terminated nanowires was then exposed to avidin.

Figure 12 shows optical and fluorescence microscope images of a Au/Ni/Au nanowire conjugated with fluorescently labeled avidin. The selective functionalization of the nanowires can be demonstrated by exposing biotin-terminated Au/Ni/Au nanowires to Neutra Avidin tetramethyl rhodamine (NATR). The fluorescence image confirms that the biotin-terminated thiol is attached only to the gold

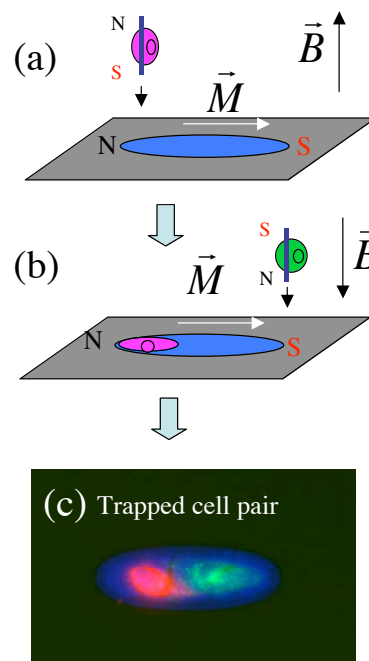


Figure 11. Heterotypic cell trapping. (a) Vertical field directs nanowires and cells to North pole of ellipsoidal hole in a magnetic film. (b) Reversing field directs second cell type to South pole of hole. (c) Composite fluorescence image of a trapped cell pair.

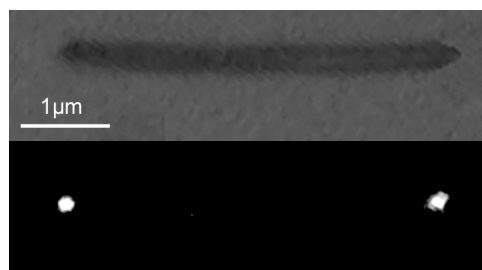


Figure 12. (Top) Light microscope image of a 300 nm diameter and 4.5 μm long Au/Ni/Au nanowire where the gold end-segments have been functionalized with biotin-terminated thiol and NeutraAvidin tetramethylrhodamine conjugate (NATR) (bottom) Corresponding fluorescence image showing that avidin is bound specifically to the Au end-segments.

end-segments.

Self-assembly experiments were performed in the following way. A suspension of nanowires with biotin-terminated end-segments (B-B) was injected into a suspension containing nanowires with avidin-terminated end-segments (A-A) in a shaker. The time dependence of the chain length distribution was obtained by extracting small aliquots of the suspension and analyzing the images in an optical microscope. The chain length is defined as the number of nanowires in a chain.

Figure 13 shows the average chain length L_{av} versus time for three experiments with concentrations of avidin-terminated and biotin-terminated nanowires ($n_{A-A} = n_{B-B}$) from $2.5 \times 10^6 \text{ cm}^{-3}$ to $6.25 \times 10^7 \text{ cm}^{-3}$. The average chain length increases with time and is largest for the highest nanowire concentration.

The end-to-end self-assembly of nanowires reported here is similar to the problem of step polymerization. The polymerization of two monomers A-A and B-B, each with two reaction sites was considered by Flory. The average chain length L_{av} is given by,

$$L_{av} = \frac{1}{1-p} = L_0 + n_0 kt$$

where n_0 is the total number of building blocks ($n_0 = n_{A-A} + n_{B-B}$), k is the rate constant associated with the reaction of an avidin-terminated end-segment (A) with a biotin-terminated end-segment (B), L_0 is the initial chain length, and p is the extent of reaction (or polymerization) defined as the ratio of the number of reacted end-segments of one type (e.g. A) to total number of end-segments of that type initially present.

The time dependence of the average chain length shown in Fig. 3(a) shows good agreement with Flory's model for step polymerization. The solid lines show least squares fits for the three experiments with slopes of $6.53 \pm 2.03 \times 10^{-5} \text{ s}^{-1}$, $5.72 \pm 0.35 \times 10^{-4} \text{ s}^{-1}$, and $1.41 \pm 0.16 \times 10^{-3} \text{ s}^{-1}$. From Eq. (1) we obtain the rate constant for end-to-end binding of $k = 1.2 \pm 0.1 \times 10^{-11} \text{ cm}^3 \text{ s}^{-1}$.

From the rate constant we can calculate the average collision time from $\tau = 1/N_0 n_0 k$ where N_0 is the total number of nanowire building blocks in the system. In our experiments $V = 1 \text{ mL}$ and the collision time decreases from 3.3 ms for a total nanowire density $n_0 = 5 \times 10^6 \text{ cm}^{-3}$ ($n_{A-A} = n_{B-B} = 2.5 \times 10^6 \text{ cm}^{-3}$) to 5.3 μs for $n_0 = 1.25 \times 10^8 \text{ cm}^{-3}$ ($n_{A-A} = n_{B-B} = 6.25 \times 10^7 \text{ cm}^{-3}$). The rate constant and collision time are also dependent on

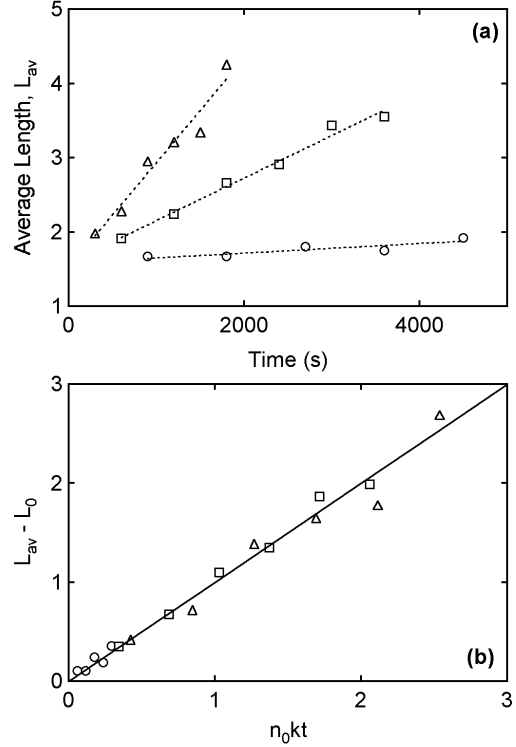


Figure 13. (a) Average chain length versus time for three experiments with initial nanowire concentrations of $n_{A-A} = n_{B-B} =$ (o) $2.5 \times 10^6 \text{ cm}^{-3}$, (□) $2.5 \times 10^7 \text{ cm}^{-3}$, and (Δ) $6.25 \times 10^7 \text{ cm}^{-3}$. (b) The average nanowire chain length normalized versus $n_0 kt$ for three experiments using $k = 1.2 \times 10^{-11} \text{ cm}^3 \text{ s}^{-1}$.

{1}

agitation. In other experiments we have shown that the rate constant increases with increasing agitation rate.

Figure 13 shows the average chain length from the three experiments replotted versus n_0kt using a rate constant $k = 1.2 \times 10^{-11} \text{ cm}^3 \text{ s}^{-1}$ and $L_0 = 1.5$. The experimental results collapse onto a universal curve consistent with Eq. (1). The intercept of $L_0 = 1.5$ is due to the fact that there is some binding that occurs on injecting biotin-terminated nanowires into avidin, even though there is a large excess of avidin. Although the nanowires are more than three orders of magnitude larger than typical molecular monomers, these results illustrate that the dynamics of end-to-end assembly of nanowires can be described by the collision model derived for step polymerization.

Magnetic Orientation of Tethered Nanowires. In addition to directing the spatial location and placement of building blocks, the subsequent ability to manipulate the building blocks is equally important. We have demonstrated that tethered nanowires can be oriented with an external magnetic field. Two segment Ni/Au nanowires with biotin-terminated gold segments were attached to avidin-terminated stripes on a gold surface. After anchoring the nanowires to the stripes through the avidin linkage, a magnetic field can be used to align the nanowires, as shown in Figure 14.

The aspect ratio of the nickel segments is about 50 and hence the magnetic easy axis is parallel to the wire axis. When a magnetic field was applied parallel to the tracks, the nanowires rotated so that the nickel segments were aligned parallel to the field, as shown in Figure 14. Similarly, when the field was applied perpendicular to the tracks, the nanowires rotated to be parallel to the field and perpendicular to the tracks. Fluorescence images confirmed that the nanowires were still anchored within the rhodamine-labeled avidin patterned regions.

These results illustrate molecular self-assembly and external manipulation of multifunctional magnetic nanowires in spatially localized regions using a microfluidic-based approach combined with selective surface functionalization. This approach has potential for applications ranging from self-assembly of intricate macrostructures to biosensors that utilize protein-based nanoscale switches (*Publication 9*).

Nanowire scaffolds in suspension created by AC electric fields We have developed a highly versatile and efficient method for assembling nanowires in suspension into various

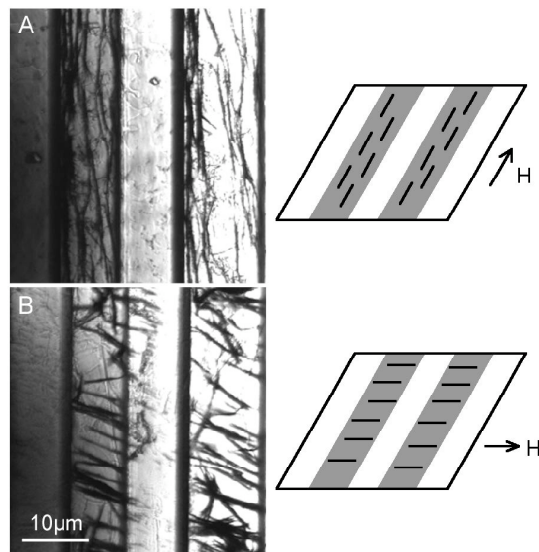


Figure 14. (a) Light microscope image of two-segment Au/Ni biotinylated nanowires tethered to patterned avidin tracks in an aqueous environment with an applied magnetic field parallel to the tracks. (b) Corresponding light microscope image with the applied magnetic field perpendicular to the tracks. The nanowires were 170 nm in diameter and 9 μm in length with 1 μm long gold segments and 8 μm long nickel segments.

nonlinear scaffolds using AC electric fields applied to strategically designed microelectrodes. We have shown the distinct effects due to the electric field (E) and electric field gradient (EFG) in aligning and transporting nanowires. The E field aligns the nanowires whereas the EFG actually transports the nanowire. We have shown that the nanowires in suspension can be assembled into specific structures according to the calculated E field distribution inherent to the electrodes (Figure 15). Randomly oriented nanowires in suspension can be rapidly assembled into extended structures within seconds. Thus, nanowires can be assembled into various structures and scaffolds by designing electrodes that generate the necessary E field distributions (*Publication 21*).

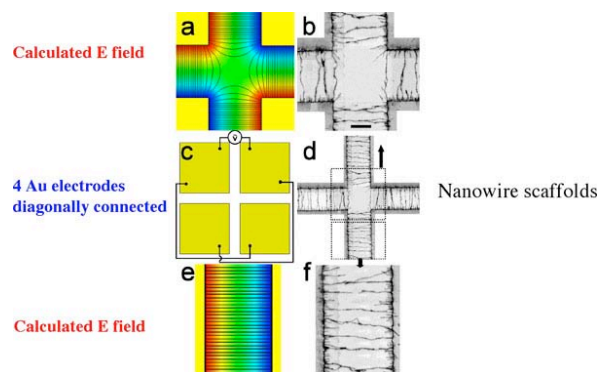


Figure 15. A cross region defined by four Au electrodes, which are connected diagonally. The nanowires rapidly assembled when AC electric field has been applied.

3.6 Drug and Gene Delivery

The goal of gene therapy is to introduce foreign genes into somatic cells to supplement the defective genes or provide additional biological functions. Gene transfer can be performed using either viral or synthetic non-viral delivery systems. While viral vectors exhibit high efficiency, synthetic transfection systems provide several advantages including ease of production and reduced risk of cytotoxicity and immune responses. Much of the poor transfection efficiency of non-viral vectors stems from the difficulty of controlling their properties at the nanoscale. We have developed a novel non-viral delivery system based on nanorods that can simultaneously bind compacted DNA plasmids and target cell receptors for enhanced internalization. Both in vitro and in vivo studies have demonstrated the potential of this versatile gene delivery system.

Gene therapy aims to introduce DNA into cells for the purpose of supplementing dysfunctional genes or introducing new functionalities. Achieving efficient gene delivery into a target cell population or tissue without causing associated toxicity is critical to the success of gene therapy. Although viral vectors such as adenovirus, lentil virus, influenza virus, and adeno-associated virus are efficient in transfecting cells, their toxicity and immunogenicity remain severe limitations.

As alternatives to viruses, non-viral vectors such as liposomes and polymers have been increasingly studied to overcome this long-term safety issue. In contrast, inorganic gene carriers have received limited attention in the gene therapy community. Gold nanoparticles with bound DNA are used in particle bombardment-mediated gene transfer. While this gene gun technology may be effective in transfecting cells in the skin for genetic immunization, it has limited utility in general gene transfer applications involving internal organ transfection.

To be effective, non-viral vectors must gain entry into the target cells and then release the condensed plasmid into the cytoplasm for translocation into the nucleus. To date, particle-based vectors have been formulated by using polycationic polymers or

lipids to condense DNA into nano-complexes that can be internalized by cells. The size of these nano-complexes is typically difficult to control and widely dispersed. Targeting ligands can be conjugated to the carrier or complexes either pre- or post- complexation with the DNA, although the carrier-conjugation might alter the properties of the complexes to an extent difficult to predict or manage. Once internalized into the cell, release of the DNA from the complexes may also become a rate-limiting step. To optimize these different aspects in designing an effective non-viral gene delivery system remains a major challenge in the field.

We first demonstrated transfection using bi-functional Au/Ni nanorods 100 nm in diameter and 200 nm in length with 100 nm gold segments and 100 nm nickel segments. Using molecular linkages that bind selectively to either gold or nickel, we have attached a cell-targeting protein, transferrin, to the gold segments through a thiol linkage, and DNA to the nickel segments through a carboxylate linkage with a protonated primary amine tail group. Transferrin was one of the first proteins to be exploited for receptor-mediated gene delivery since all metabolic cells internalize iron via receptor-mediated endocytosis of the transferrin-iron complex. A rhodamine tag on the transferrin provided a mechanism for confirmation of internalization and intracellular tracking of the nanorods. Confirmation of the selective binding of transferrin and plasmid was obtained by fluorescence microscopy.

To evaluate the gene delivery potential of these dual functionalized Au/Ni nanorods, *in vitro* transfection experiments were performed on the Human Embryonic Kidney (HEK293) mammalian cell line with the GFP and luciferase reporter genes, respectively. Confocal microscopy and electron microscopy confirmed successful transfection with both reported genes. Transmission electron microscope images showed that nanorods were located in vesicles or the cytoplasm but not the nucleus. This suggests that transfection is due to plasmids released or cleaved from the nanorods prior to nuclear entry.

Figure 16 summarizes the transfection experiments for the luciferase reporter gene. A significantly higher fraction of cells expressed luciferase when transfected with plasmid-nanorods than with naked DNA. Nanorods with DNA and transferrin were about 4 times more efficient than nanorods with DNA alone. Addition of chloroquine to nanorods with transferrin further improved GFP expression by a factor of about 2. The fact that chloroquine enhances transferrin-mediated transfection suggests that receptor-mediated endocytosis is involved. Chloroquine may also enhance transfection by protecting against DNA degradation. [Publication 6]

Size dependence of transfection efficiency To further understand the potential of these nanorods in intracellular delivery, we have performed a systematic study to examine the

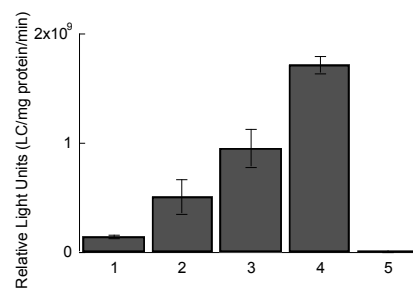


Figure 16. Luciferase expression for 1. nanorod-plasmid complex, 2. nanorod-plasmid/transferrin complex, 3. nanorod-plasmid/transferrin complex incubated with 100 μM chloroquine, 4. Lipofectamine (positive control) and 5. naked DNA (negative control).

effects of size, targeting ligand, and magnetism of these nanorods on gene delivery in vitro.

Nanorods 100 nm in diameter and with length varying from 100 to 6,000 nm, equally divided between gold and nickel segments, were synthesized by electrochemical deposition. The following size discussion therefore refers to length variation. For 100 nm-long nanowires, the immobilization of transferrin resulted in an 11.5 fold increase in transfection efficiency against HEK293 cells compared to nanowires without the transferrin. For 319 nm nanowires, this increase fell to 1.8 fold. The attachment of transferrin to nanowires larger than this did not result in any significant increase in transfection efficiency. A broad decrease in transfection was observed with increasing nanowire size. Nanowires 1 μm long were 15.6 fold less efficient than the 100 nm nanowires. Because the dose of the nanowires was kept constant (1 μg DNA), translating to fewer number of wires as the length goes up, the decrease is partially due to a lower distribution of the nanowires over the cell culture dish.

To take advantage of the magnetic properties of the nanowires, we investigated the possible enhancement effect of magnetofection. When a NdFeB magnet was applied to the bottom of a culture dish containing 100 nm nanorods during the 4hr transfection period, a 3-fold increase in transfection efficiency was observed. TEM sections did not reveal any difference in the mechanism of uptake, indicating that this increase in expression was due to accelerated sedimentation of the vectors to the surface of the cell.

To prepare for the gene gun delivery of these nanowires we examined the transfection efficiency as a function of size and pressure in vitro. In contrast to incubation with nanowires, gene gun delivery with increasing nanowire size from 100 nm to 1 micron at a constant pressure of 250 psi resulted in higher transfection efficiency. However, increasing the length of nanowires above 1 μm began to produce lower transfection efficiencies because of toxicity to the cells. Increasing pressure of the delivery of 100 nm nanowires resulted in decreasing the viability of HEK293 cells from 82% (250 psi) to 48% (400 psi) to 14% (600 psi). In summary, this study reveals the relationship between size, uptake mechanism, cytotoxicity, magnetic force, and in vitro transfection efficiency of these nanorods.

Genetic immunization with nanowires We evaluated the nanorods in genetic immunization using gene gun delivery. We evaluated the CD4+ antibody and CD8+ T-cell responses from bombardment of nanorods delivering the model antigen ovalbumin protein or plasmid encoding the ovalbumin. We attached plasmids and/or the antigen, ovalbumin, to the different segments, as described previously. A small proportion of the primary amine groups of ovalbumin were converted to sulfhydryl groups. The ovalbumin was then bound to the gold segments of the nanorods through a thiolate linkage. Plasmids encoding ovalbumin (pcDNA3-OVA7) or control plasmids with blank inserts (pcDNA3) were also attached to the nanowires in a manner described previously.

The antibody responses from the bloodstream and CD8+ T-cell responses from the spleen were measured from C57BL/6 mice vaccinated with the nanorod/plasmid or nanorod/antigen formulations. In addition, we compared these responses to those generated by the industrially optimized gold particle formulations, the standard in the field of gene gun-mediated genetic immunization. For antigen/microcarrier formulations, the gold particles generated a 7-fold higher CD8+ T-cell response than the nanorods. In contrast, for the antibody response, the nanorods produced a 7-fold higher response in

comparison with the 1.6 μm gold particles (Figure 17). To evaluate the benefit of the nanorods multifunctionality, pcDNA3, the blank molecular construct without the antigen gene, was bound to the nickel segments of the nanorods in conjunction with the ovalbumin-SH antigen on the gold segments. In control experiments, pcDNA3 bound to the nanorods alone generated very low or no antibody and CD8⁺ T-cell responses.

Delivering plasmids encoding ovalbumin by both nanorods and gold particles generated stronger antibody and CD8⁺ T-cell responses than the ovalbumin antigen alone. Gene gun delivery of antigens can directly enter and prime dendritic cells, but the delivery of plasmids encoding the

antigen probably enhances the overall response because in addition to directly priming the dendritic cells, it may also transfect keratinocytes. The keratinocytes then produce antigens that once released can cross-prime more dendritic cells to further the overall immune response.

In summary, we have shown that these versatile nanorods generate strong antibody and CD8⁺ T-cell responses and therefore have significant potential for further development in vaccination applications. In future studies, we anticipate that aligning the nanorods within the cartridges to produce “arrow” like delivery may allow us a much more favorable penetration depth-pressure relationship in particle bombardment than the gold particles. Advantages to this would include transfecting both skin and the subcutaneous tissues for pressure modulated control over sustained or transient expression of genes and greater depths of penetration at lower pressures. The ability to add new components to the nanorods such as adjuvants and/or cytokines in controlled ratios will allow us to generate stronger immune responses than single component particles as demonstrated in this study using the CpG motif from the pcDNA3 as an immunostimulatory adjuvant to the antigen. In addition, the ability to engineer and add extra segments to the nanorods will allow for the possibility of delivering multiple agents such as RNA, antigens and DNA to the same cell for the stimulation of multiple immune responses. (*Publication 13*)

Magnetofection: We have further investigated the possibility of taking advantage of the magnetic component of the nanorods to achieve a more favorable penetration depth-pressure relationship in particle bombardment than the gold particles.

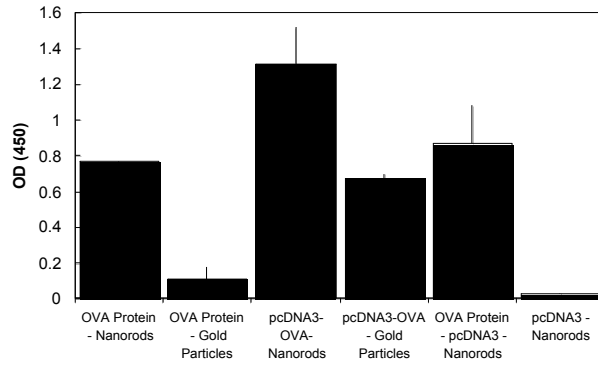


Figure 17. Ovalbumin-specific antibody responses in C57BL/6 mice immunized with various antigen or plasmid nanorod and gold particle formulations. C57BL/6 mice were immunized with control plasmid (no insert) bound to nanorods, ovalbumin antigen-nanorod formulation, ovalbumin antigen-gold particle formulation, pcDNA3-OVA-nanorod formulation, pcDNA3-OVA-gold particle formulation and ovalbumin antigen/control pcDNA3 (no insert)-nanorod formulation via a gene gun. Serum samples were obtained from immunized mice 21 days after the initial vaccination. The presence of the ovalbumin-specific antibody was detected by ELISA using serial dilution of sera. The results from the 1:1000 dilutions are presented showing the mean absorbance (A450 nm) \pm SE.

We first studied magnetic field effects on in vitro transfection of HEK293 cells (Figure 18). When a NdFeB magnet was applied to the bottom of a culture dish containing 100nm nanowires during the 4hr transfection period, a 3-fold increase in transfection efficiency was observed. TEM sections did not reveal any difference in the mechanism of uptake, indicating that this increase in transgene expression was due to accelerated sedimentation of the vectors to the surface of the cell. When transferrin was added to the 100 nm nanowires without a magnetic field, we

observed a 4-fold increase in transfection. The combination of transferrin immobilization and a magnetic field resulted in a 5.25 fold increase in transfection. A possible explanation for why transferrin does not improve transfection significantly in the presence of a magnetic field is that the magnetic field may be orientating the nanowires to face towards the cell surface with the nickel portion, which is the DNA-binding segment, thus somewhat negating the effects of transferrin in targeting the transferrin receptor.

Although the above study demonstrates the possible benefit of magnetofection with these nanowires, it also illustrates that a greater control over the magnetic field gradients to orient the nanowires would be needed to enhance the transfection further. We hypothesized that a ring magnet placed at the outlet of the Helios gene gun would orient the nanowires and improve their penetration depth. To facilitate imaging, we first developed a technique to label nanowires with quantum dots. The nanowires were then shot into an agarose gel. Figure 19 shows the vertical cross-sectional image of a 2% agarose gel imbedded with nanowires delivered by the Helios gene gun at a 400 psi He gas pressure.

The agarose gel was then vertically cut with a blade and placed

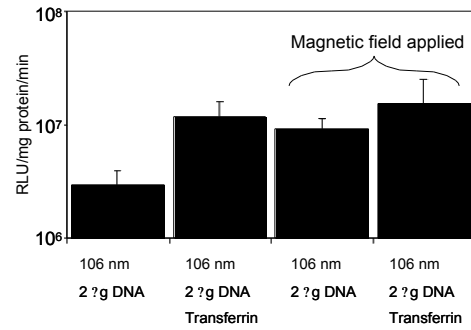


Figure 18. Effect of magnetic field on enhancing transfection efficiency of DNA-immobilized Au-Ni nanorods. A NdFeB magnet was placed at the bottom of a culture dish during the incubation of nanorods (without the use of gene gun

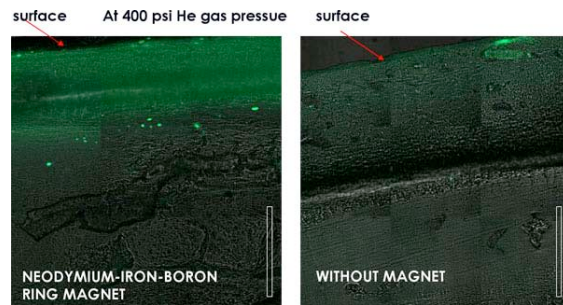


Figure 19. Vertical cross-sectional image of a 2% agarose gel imbedded with nanorods delivered by the Helios gene gun at a 400 psi He gas pressure.

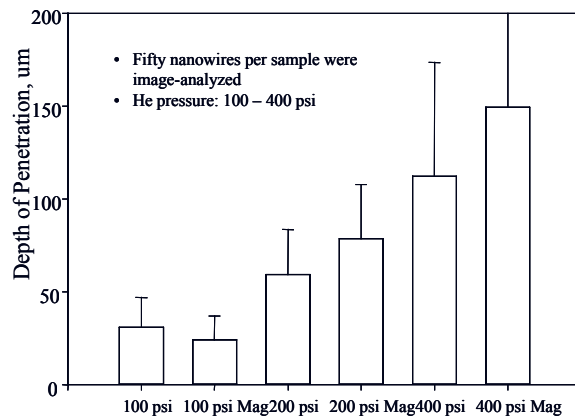


Figure 20. Enhancement of penetration by nanowires into agarose gel during gene gun delivery resulting from magnetic alignment of nanowires during flight.

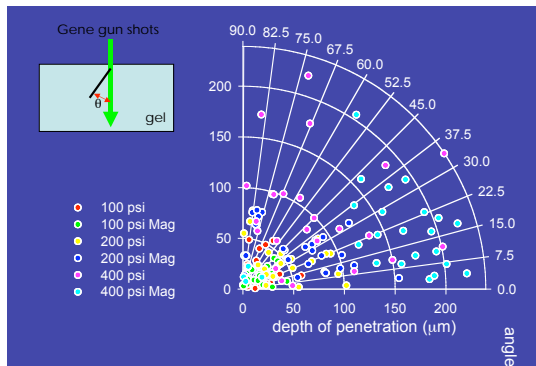


Figure 21. Angular distribution of nanowires in agarose.

placement of the nanorods in the agarose gel. The more detailed analysis shows that the ring magnet improved the penetration and orientation of the nanorods at the same injection pressure.

3.7 Magnetic detection of nanowires

As part of the development of magnetic nanowires for biomagnetics, it is important to evaluate and explore magnetic sensing strategies for the wires. Development of these techniques is relevant for our program for the detection and monitoring of cell-manipulation techniques and for magnetic detection of cell transfection. More generally, the advancement of wire-sensing technology will enable wider applications of these novel magnetic nanostructures. We are pursuing two approaches for nanowires sensing: the first uses giant-magnetoresistance (GMR) spin-valve sensors fabricated by NVE, Inc., a company participating in the DARPA BioMagnetICs program. The second approach uses magnetic tunnel junction (MTJ) sensors fabricated at Brown University, and by our sub-contractor, Micromagnetics, Inc.

Figure 22 shows the successive detection of two 5 μm Ni nanowires in liquid suspension by a NVE GMR device. This has a 100 μm x 100 μm active area, with the sensors configured in a Wheatstone bridge. The sensitivity is approximately 400 $\mu\text{V}/\text{mA}$ G. It is clear that single nanowire detection is possible. We also find a linear response vs coverage of the sensor (*Publication 10*).

The Brown University team worked with scientists at Micro Magnetics to demonstrate the use of highly sensitive magnetic tunnel junction (MTJ) sensors for the detection of individual micron-sized magnetic labels. By integrating the MTJ sensor into a microfluidic channel, we were able to detect the presence of moving superparamagnetic beads (Dynabeads M-280) in real time by direct measurement of the magnetic dipole fields associated with single beads. The dipolar fields of a single bead were sufficient to obtain a signal of 80 μV with signal to noise ratio of 24 dB in an

on a thin cover glass. The quantum dot conjugated nanorods were visualized under a confocal microscope at an excitation wavelength of 405 nm and an emission wavelength of 420 nm. An optical sectioning was performed at every 5 μm , and each slice was analyzed for the number and orientation of the nanorods. Figure 20 shows the nanowire penetration as a function of injection pressure and with or without a ring magnet placed at the outlet of the gene gun.

Figure 21 shows the individual

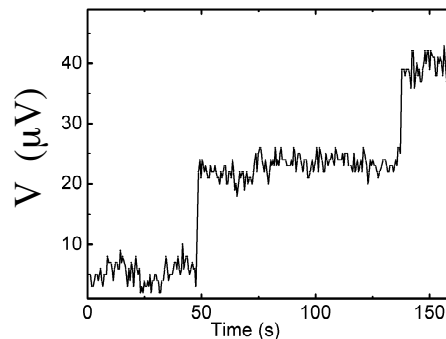


Figure 22. Time trace from a GMR sensor showing the detection of two 5 μm Ni nanowires ($\mu \sim 2 \times 10^{-10}$ emu).

applied field of 15 Oe. Our data show conclusively that MTJ sensors are very promising candidates for future applications involving the accurate detection and identification of biomolecules with magnetic labels. (*Publication 17*).

To be better suitable for biomagnetic detection, MTJ serial array sensors were fabricated for real-time capture the movements of magnetic beads/wires above the sensor area. MTJ serial array is a promising design because the array size and chip layout is more compatible with current standard DNA microarray technique. We have fabricated four 64-MTJ serial arrays (Figure 23) on a single chip, with MR value of 9.5% and high sensitivity. We have also demonstrated biological compatibility of these devices.

To detect the magnetic signal from a single nanowire, a magnetic tracking bar (2000Å CoPtCr) was patterned close to the MTJ sensor area. In addition to localizing the nanowires, the magnetic bar also provides a field to bias the MTJ sensor. A micro-channel (300 μm width) was covered above the sensor area, nanowires in solution was introduced into channel and captured by the magnetic bar. The detection of single nanowire becomes possible when they are captured close to the MTJ sensor (Figure 24).

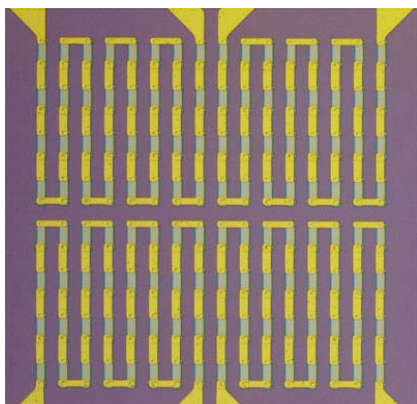


Figure 23. 64-MTJ serial sensor array.

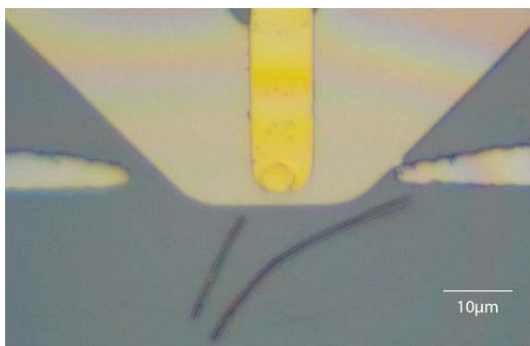


Figure 24. MTJ sensor with magnetic tracking bars for detecting single nanowires.

3.8 Multifunctional nanorings

We have worked to extend the concept of asymmetric, multifunctional magnetic nanoparticles for biomagnetics to other particle geometries. One promising geometry is the nanoring, which, despite its unique attributes, has not been significantly explored because of the inherent difficulties in large-scale fabrication. We have recently developed a new method of using self-assembly of two-dimensional nanoparticle arrays as templates for the fabrication of a large number ($>10^{10}$) of sub-100 nm nanorings over a macroscopic area (2cm x 2 cm) with high areal density (45 rings/ μm^2), as shown in Fig25. These nanorings can be made from wide variety of materials, and can easily be made from multiple, layered components. With the success of this new method, we can now address a host of interesting problems capitalizing on the nanoring geometry, and their unique magnetic properties. For example, a two-layer ring could be functionalized top and bottom with different ligands to achieve multifunctionality. The rings can be made into high-density arrays for trapping or sensing purposes, or used in suspension for a variety of cell manipulation applications (*Publications 12, 22*).

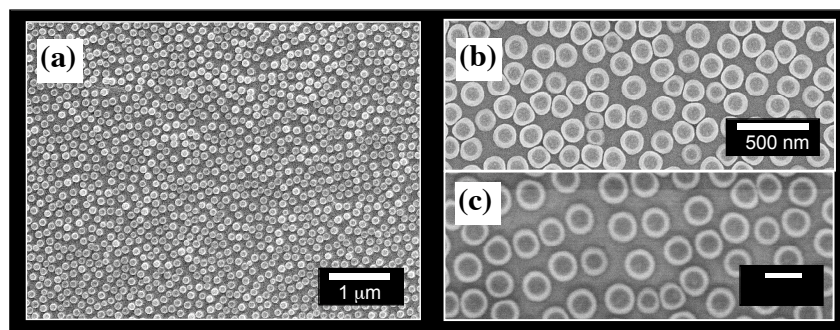


Figure 25. SEM images of Co nano-rings made from 100 nm polystyrene nanospheres. Rings inner diameter is 100 nm, and outer diameter is 140 nm. (a) Areal density is 30 Gbits/in²; (c) Image using SEM's composition detector.

4. Personnel supported by or affiliated with the project:

Faculty:

Chia-Ling Chien,	Department of Physics and Astronomy
Kam Leong	Department of Biomedical Engineering
Gerald. J. Meyer	Department of Chemistry
Daniel H. Reich	Department of Physics and Astronomy
Peter C. Searson	Department of Materials Science and Engineering
Christopher S. Chen,	Department of Bioengineering, University of Pennsylvania
Gang Xiao	Department of Physics – Brown University

All participating faculty received salary support at the rate of one calendar month per year to support their efforts on this project

Postdoctoral Fellows:

	Current Position
Alexandre Anguelouch	JHU
Kiran Bhadriraju	Research Staff, NIST
Aliasger Salem	Assistant Professor, University of Iowa
Hyuk Sang Yoo	JHU

Graduate Students:

	Current Position
Laura Bauer	Ph.D., 2003; Postdoc, Ames Lab, CA
Nira Birnbaum	Ph.D., 2005 USPTO
Min Chen	Ph.D., 2005 Giner, Inc.
Edward Felton	JHU
Amanda Fond	JHU
Anne Hultgren	Ph.D., 2005 Analyst, Booz-Allen Hamilton, Inc.
Chungxin Ji	Ph.D., 2003. Technical Staff, General Motors
Xiaoyong Liu	Ph.D., 2005; Postdoc, Brown University
Weifeng Shen	Brown University
Monica Tanase	Ph.D., 2004. Postdoc, Columbia University.
Jami Valentine	Ph.D., 2006 USPTO

5. Publications:

1. L. A. Bauer, D. H. Reich, and G. J. Meyer, "Selective Functionalization of Two-Component Magnetic Nanowires," *Langmuir* **19**, 7043 (2003).
2. N. S. Birenbaum, C. S. Chen, D. H. Reich, and G. J. Meyer, "Selective Non-Covalent Adsorption of Protein to Bifunctional Metallic Nanowire Surfaces," *Langmuir* **19**, 9580 (2003).
3. M. Chen, L. Sun, J. E. Bonevitch, D. H. Reich, C. L. Chien, and P. C. Searson, "Tuning the response of magnetic suspensions," *Appl Phys. Lett.* **82**, 3310 (2003).
4. D. H. Reich, L. A. Bauer, M. Tanase, A. Hultgren, C. S. Chen, and G. J. Meyer "Biological Applications of Multifunctional Magnetic Nanowires (invited)," *J. Appl. Phys.* **93**, 7275, (2003).

5. A. Hultgren, M. Tanase, C. S. Chen, G. J. Meyer, and D. H. Reich, "Cell Manipulation using Magnetic Nanowires," *J. Appl. Phys.* **93**, 7554 (2003).
6. A. K. Salem, P. C. Searson, and K. W. Leong "Multifunctional Nanorods for Gene Delivery, *Nature Materials*, **2**, 668 (2003).
7. L. A. Bauer, N. S. Birenbaum, and G. J. Meyer, "Biological Applications of High-Aspect Ratio Nanoparticles," *J. Mater. Chem.* **14**, 517 (2004).
8. A. Salem, J. Chao, K. Leong, and P. C. Searson, "Receptor-mediated self-assembly of multi-component magnetic nanowires, *Adv. Mater.* **16**, 268 (2004).
9. A. K. Salem, M. Chen, J. Hayden, K. W. Leong, and P. C. Searson "Directed Assembly of Multi-Segment Au/Pt/Au Nanowires," *Nano Lett.* **4**, 1163-1165 (2004).
10. A. Anguelouch, D. H. Reich, C. L. Chien, and M. Tondra, "Detection of Ferromagnetic Nanowires using GMR Sensors," *IEEE Trans. Mag.* **40**, 2997 (2004).
11. A. Hultgren, M. Tanase, C. S. Chen, and D. H. Reich, "High-yield cell separations using magnetic nanowires," *IEEE Trans. Mag.* **40**, 2988 (2004).
12. F. Q. Zhu, D. L. Fan, X. C. Zhu, J. G. Zhu, R. C. Cammarata, and C. L. Chien, "Ultrahigh-Density Arrays of ferromagnetic nanorings on macroscopic areas," *Adv. Mater.* **16**, 2155 (2004).
13. A. K. Salem, C. F. Hung, T. W. Kim, T. C. Wu, P. C. Searson, and K. W. Leong, "Multi-component nanorods for vaccination applications," *Nanotechnology* **16** (4): 484-487 (2005).
14. L. Sun, Y. Hao, C. L. Chien, and P. C. Searson, "Tuning the properties of magnetic nanowires," *IBM J. Res. Dev.* **49**, 79-102 (2005).
15. A. Hultgren, M. Tanase, E. J. Felton, K. Bhadriraju, A. K. Salem, C. S. Chen, and D. H. Reich, "Optimization of Yield in Magnetic Cell Separations Using Magnetic Nanowires of Different Lengths," *Biotech. Prog.* **21**, 509-515 (2005).
16. M. Tanase, E. J. Felton, D. S. Gray, A. Hultgren, C. S. Chen, and D. H. Reich "Assembly of multicellular constructs and microarrays of cells using magnetic nanowires," *Lab on a Chip* **5**, 598-605 (2005).
17. W. Shen, X. Liu, D. Mazumdar, and G. Xiao, "In situ detection of single micro-sized magnetic bead detection using magnetic tunnel junction sensors," *Appl. Phys. Lett.* **86**, 253901 (2005).
18. M. Chen, L. Guo, R. Ravi, and P. C. Searson, "Kinetics of Receptor Directed Assembly of Multisegment Nanowires," *J. Phys. Chem.* **110**, 211-217 (2006).
19. A. M. Fond, N. S. Birenbaum, E. J. Felton, D. H. Reich, and G. J. Meyer "Preferential Noncovalent Immunoglobulin G Adsorption onto Hydrophobic Segments of Multi-Functional Metallic Nanowires," To appear in *Journal of Photochemistry and Photobiology A: Chemistry*.
20. E. J. Felton and D. H. Reich, "Biological Applications of Multifunctional Magnetic Nanowires," for inclusion in *Biomedical Applications of Nanotechnology*, to be published by John Wiley & Sons in 2006.
21. D. L. Fan, F. Q. Zhu, R. C. Cammarata, and C. L. Chien, "Manipulation of nanowires in suspension by ac electric fields," *Appl. Phys. Lett.* **85**, 4175-4177 (2004).

22. F. Q. Zhu, G. W. Chern, O. Tchernyshyov, X. C. Zhu, J. G. Zhu, and C. L. Chien, "Magnetic bistability and controllable reversal of asymmetric ferromagnetic nanorings," *Phys. Rev. Lett.* **96**, 027205 (2006).

6. Interactions/Transitions:

a. Participation/presentations at meetings, conferences, seminars, etc.:

1. D. H. Reich, "Multifunctional Magnetic Nanowires," Invited presentation, International Conference on Fine Particle Magnetism, Pittsburgh, PA, August, 2002.
2. M. Tanase, "Magnetic nanowires, tools for cellular manipulation," NanoBioTech Conference, Columbus, OH, September, 2002.
3. D. H. Reich, "Biological Applications of Multifunctional Magnetic Nanowires." Invited oral presentation at Magnetism and Magnetic Materials Conference, Tampa, FL, November, 2003.
4. A. Hultgren, "Cell Manipulation using Magnetic Nanowires." Contributed oral presentation at Magnetism and Magnetic Materials Conference, Tampa, FL, November, 2003.
5. M. Chen, "Micromagnetic behavior of electrodeposited Ni/Cu multilayer nanowires, Contributed oral presentation at Magnetism and Magnetic Materials Conference, Tampa, FL, November, 2003.
6. P. C. Searson, "Tailoring the Properties of Multilayer Nanowires," Invited oral presentation at APS March Meeting, Austin, TX, March, 2003.
7. M. Tanase, "Directed assembly of cells with magnetic nanowires," Contributed oral presentation at APS March Meeting, Austin, TX, March, 2003.
8. A. Hultgren, "Magnetic cell separation with electrodeposited nanowires," Contributed oral presentation at APS March Meeting, Austin, TX, March, 2003.
9. N. Birenbaum, "Selective Non-Covalent Adsorption of Protein to Bifunctional Metallic Nanowire Surfaces." Contributed poster presentation at Microbiology Society Meeting, New York, NY, July, 2003.
10. DARPA BiomagnetICS Program Kickoff Meeting, July 2003: Attended by C. S. Chen, K. Leong, G. J. Meyer, D. H. Reich, A. Anguelouch, A. Salem, L. A. Bauer, and A. Hultgren. Posters were presented by Anguelouch, Salem, Bauer, and Hultgren. An oral overview of our program was presented by Reich.
11. Salem, A.K., P.C. Searson, and K.W. Leong, "Multifunctional Nanorods for Gene Delivery," MRS Symposium, Boston, 2003
12. K.W. Leong, A.K. Salem, and P.C. Searson, "Nanorods for non-viral gene delivery," 2nd International Conference on Materials Advanced Technology, Singapore, December, 2003
13. K.W. Leong, R.J. Sung, T. Kiang, Salem, A.K., and P.C. Searson, C.F. Hung, "Delivery aspects of DNA vaccination," Keystone Conference on Vaccines, Keystone, Colorado, January, 2004.
14. A. Hultgren, "Cell Separations Using Magnetic Nanowires," Contributed oral presentation, 9th Joint MMM/Intermag Conference, January, 2004.

15. K.W. Leong, J. Wen, H.Q. Mao, T. Kiang, Salem, A.K., and P.C. Searson, C.F. Hung, "Nanoparticles in biomedical applications," NIH Workshop on Interface of Nanotechnology and Cancer Imaging," Bethesda, Maryland, January, 2004
16. D. H. Reich, "Multifunctional magnetic nanowires for biotechnology applications," Invited oral presentation, Photonics West (SPIE International Conference), San Jose, CA, January, 2004.
17. D. H. Reich, "Magnetic nanoparticles and spintronics in biology and biotechnology: current uses and new approaches," Spintronics Tutorial, American Physical Society March Meeting, Montreal, Canada, March, 2004.
8. D. H. Reich, "Biological Applications of Multifunctional Magnetic Nanowires" Invited oral presentation, 2nd Annual Research, Technologies, and Applications in Biodefense Conference, Washington, DC, August, 2004.
9. P. C. Searson, "Synthesis And Assembly of Multifunctional Nanowires" Invited oral presentation, Particles 2004 Orlando, FL, March, 2004
10. P. C. Searson, "Self-Assembly of Multifunctional Particles For Nanostructures" Physics Seminar, NASA Goddard Space Flight Center, Laurel, MD, March, 2004.
18. P. C. Searson, "Electrochemical Synthesis of Multifunctional Building Blocks For Nanosystems" " Invited oral presentation, 227th ACS National Meeting, Anaheim, CA, March, 2004.
19. D. H. Reich, "Multifunctional Magnetic Nanowires for Biotechnology and Biomagnetics Applications," Invited oral presentation, Material Research Society Meeting, San Francisco, CA, March, 2005
20. D. H. Reich, "Magnetic Nanoparticles for Biology and Biotechnology: Current Uses and New Approaches," Michigan State University, April, 2005.
21. E. J. Felton, A. Hultgren, M. Tanase, D. H. Reich, and C. S. Chen, "Cell Structure Assembly with Magnetic Nanowires, Contributed oral presentation, American Physical Society March Meeting, Los Angeles, CA, March, 2005.
22. M. Chen and P. C. Searson, "Multicomponent Nanowires Assembled by Biological and Magnetic Interactions, " Oral presentation, Material Research Society Meeting, San Francisco, CA, March, 2005.
23. P. Searson, "Multifunctional nanoparticles," G. E. Global Research, Schenectady, NY, April, 2005.
24. D. Reich, "Cell Manipulation and Sub-Cellular Force Measurements Using Magnetic Nanowires," Symposium on Mining the Biology-Physics Interface, Johns Hopkins University, January, 2006.

b. Consultative and advisory functions to other laboratories and agencies:

In 2004, D. Reich provided magnetic microarrays to Dr. Lloyd Whitman's group at the Naval Research Laboratory for use in their DARPA-funded investigations of magnetotactic bacteria for Biomagnetics applications.

c. Transitions: None.

7. New discoveries, inventions, or patent disclosures.

1. A. K. Salem, K. Leong, and P. C. Searson, "Nanorods for non-viral gene therapy." US Patent application 20050101020, filed June 24, 2004.

2. D. H. Reich, M. Tanase, and C. S. Chen, “Method and Magnetic Microarray System For Trapping and Manipulating Cells,” Patent filed by Johns Hopkins University, US Patent application 10/885,275, PCT Serial No.: PCT/US04/21688 Filed July 6, 2004.

8. Honors/Awards:

1. Laura Ann Bauer (Department of Chemistry, JHU) was awarded an Ada Sinz Hill Fellowship for exceptional progress in her thesis research (2003).
2. Professor Chia-Ling Chien was awarded the 2004 Adler Lectureship of the American Physical Society.